Mass transfer behavior in membrane distillation: effect of temperature, membrane material, flow regime, and membrane pore size

Mekdimu Mezemir Damtie[1], Bongchul Kim[2], Kwang-Duck Park[2], Yun Chul Woo[2], Ho Kyong Shon[3], and June-Seok Choi[1,2,*]

[1]Department of Construction Environment Engineering, University of Science & Technology, (34113) 217, Gajeong-ro, Yuseong-gu, Daejeon, Republic of Korea

[2]Department of Land, Water and Environment Research, Korea Institute of Civil Engineering and Building Technology, (Daehwa-Dong) 283, Goyang-Si, Gyeonggi-Do,10223, Republic of Korea

[3]Centre for Technology in Water and Wastewater, School of Civil and Environmental Engineering, University of Technology Sydney (UTS), P.O. Box 123, Broadway, NSW 2007, Australia

*Corresponding author: June-Seok Choi (Email: jschoi@kict.re.kr)

Abstract

Four commercially available hydrophobic membranes (0.22 μm / 0.45 μm PVDF, 0.1 μm PP, and 0.22 μm PTFE) in direct contact membrane distillation (DCMD) apparatus were investigated in terms of the effect of fouling on the membrane distillation (MD) mass transfer coefficient and the dominant mode of mass transport phenomenon under different conditions (temperature, membrane material, flow regime, and membrane pore size). Accordingly, results confirmed that the fouling layer affects the mass transport resistance directly by resisting mass transport and indirectly by decreasing the heat transfer mechanism. In addition to the surface fouling layer, in MD, a significant quantity of particles was found to accumulate in the membrane pores. It was also observed that the contribution of Poiseuille flow to the entire mass transport phenomenon is significant at higher temperatures for larger pore size membranes. This highlights the need for careful consideration of the Poiseuille flow in the modeling and simulation of the MD mass transport process. It can be concluded that the flow rate does not affect the Poiseuille flow and cannot directly influence the entire mass transfer. Besides, this study provides systematic insight into how to develop a strategy to select the appropriate operating feed/permeate temperature fitting for our water demand and environmental conditions.

Keywords: Membrane distillation, Modeling, Mass transfer analysis, Poiseuille flow, Isoflux

1 Introduction

The increasing rate of freshwater scarcity has provoked the development of various advanced water treatment technologies. Membrane distillation (MD) is one of the promising technologies for treating water from saline seawater and highly polluted industrial wastewater. It is a thermally-driven (vapor pressure) filtration process utilizing hydrophobic micro-porous membranes to separate water vapor from hot feed water [1]. Compared to the other membrane and desalination processes, MD has various relatively interesting features in that it requires lower operating temperature (less than water boiling point) than traditional distillation technology; MD also has high recovery rate and less fouling tendency and requires less hydrostatic pressure compared to pressure driven membrane systems [2]. In addition to this, the MD process can be easily integrated with other treatment technologies and renewable energy sources to treat extremely polluted water sources (e.g. highly saline sea water, high organic strength wastewater, and wastewater containing radioactive elements). However, because this technology is in its infancy, it has not yet been well explored and still has some limitations, mainly associated with its low permeate flux. Due to a lack of full understanding of the entire mass transport phenomenon, no advanced breakthrough has been made so far toward responding to the low permeate yield. Subsequently, accurate modeling of the mass transfer mechanism through the porous hydrophobic MD membrane and through the fouling cake layer has not been precisely performed yet [3,4].

In general, the mass transport mechanism in MD applied for treating highly polluted water involves various transport resistances. The resistances from the fouling cake layer and from the membrane itself are the major resistances to be considered in the modeling and design of the MD process [5]. In order for the vapor to reach the permeate side, molecules first have to pass through the polarization layers, then through the fouling cake layer, and finally through the hydrophobic membrane (see **Fig. 1**). In addition to the mass transfer resistance in the membrane, all these layers will confer resistance to the vapor transport, which is dependent on the fouling layer characteristics such as porosity and thickness [6]. The MD flux decline and the entire mass transport process through the fouling cake layer is a controversial issue and still complex, as it mainly depend on the membrane type and the location and type of foulants deposited [7,8]. Numbers of researchers believe that an added hydraulic resistance of the fouling layer is the major reason for the flux decline in MD [3,9,10], others believe that flux reduction is from both hydraulic mass transfer resistance and from the added heat transfer resistance of the fouling layer [8,11]. However, Tan et al. [8] described neither of these resistances are significantly contributing to the flux decline. It rather described the Kelvin effect to be the major has cause for the vapor-pressure reduction.

The permeate flux amount and its quality are also directly linked to the situation, whether there is deposition inside the membrane or only on the membrane surface. A study which utilized a synthetic organic solutions has confirmed deposition on the MD membrane surface and passage of organics to the permeate side [12]. The other study using real seawater also confirmed identical mode of deposition [1]. On the other hand, it was also pointed out that there is a deposit on the membrane surface but organic molecules do not pass through the membrane as there is no wetting [13]. Another work also used saline wastewater and ground water and found significant deposition of $CaSO_4$ scale inside the membrane pores and on the membrane surface [14]. Hence,

further detailed investigation considering certain additional factors (membrane and operational parameters) has to be conducted to understand the mass transport phenomenon in the fouling layer. Various modeling and simulation studies have been carried out to describe the flux decline trend of MD under different conditions [15]. These studies considered both analytical models [16] and quasi microfiltration empirical and semi-empirical models [9,17]

After a vapor molecule has passed the fouling cake layer, mass transport through the MD membranes has its own complex feature depending on the membrane and operating parameters. Different modeling and simulation approaches have been studied to describe the mass transport through the MD membrane. These includes the Fick's law model, the dusty gas model, structural network models, and Schofield's model [18]. All these approaches have their own advantages and drawbacks. However, the dusty gas model is the easiest and most commonly applied mass transfer analysis technique applied in the modeling and simulation of the MD process [19] (see next section: theory of mass transfer in MD). In this model, the entire mass transport through the hydrophobic membrane follows both a diffusion mechanism (Knudsen, molecular, and surface diffusion) [20] and Poiseuille flow [21]. However, in most cases, the surface diffusion and Poiseuille flow models are neglected because of their minimal contribution to the mass transport process [22]; there are cases, however, in which these models might have significant importance.

The novelty of this study lies in its ability to propose new directions that indicate conditions at which the viscous/Poiseuille flow model can no longer be ignored and present a new technique for estimating the dominant mass transport mechanism in different types of membranes. Moreover, it rectifies whether higher flux variation in different membranes with identical pore sizes results from a difference in mass transfer phenomenon and addresses how the fouling cake layer can affect the MD mass transfer mechanism. In order to achieve these, the objective of this work is therefore to study the overall mass transfer mechanism in the fouling layer and through the membrane taking into consideration various operating and membrane parameters. Specifically, it investigates the mode and type of vapor transport in MD and assesses the effect of different membrane and operational parameters on the mass transfer tendency (with special consideration of the Poiseuille flow in the overall mass transport analysis). The study also addresses how the fouling layer in MD induces the mass transfer reduction. Further, this study identifies and clearly shows the role of the transmembrane thermal gradient in the mass transfer performance of the MD membrane.

2 Theory of the mass transfer in membrane distillation

The transport of vapor molecules from the feed to the permeate side involves four steps. These include resistance from feed side concentration polarization, from cake layer accumulation on the membrane surface, from the membrane body, and from distillate side polarization [23]. **Fig. 1** shows different zones of the mass resistance and an electrical mock-up of the mass transfer from the feed to distillate side, where R_{pf}, R_{fl}, and R_{pp} represent the resistances of feed side polarization, fouling layer, and permeate side polarization, respectively, and R_k, R_p, R_s, and R_o refer to resistance from Knudsen, Poiseuille, surface, and molecular type flow conditions, respectively. The overall mass transfer coefficient (B) through the membrane is then estimated as the inverse

of the total mass transport through each media(B_{fb},B_{fl},B_m, and B_{pp}), and can be expressed mathematically using **Eq. 1.**

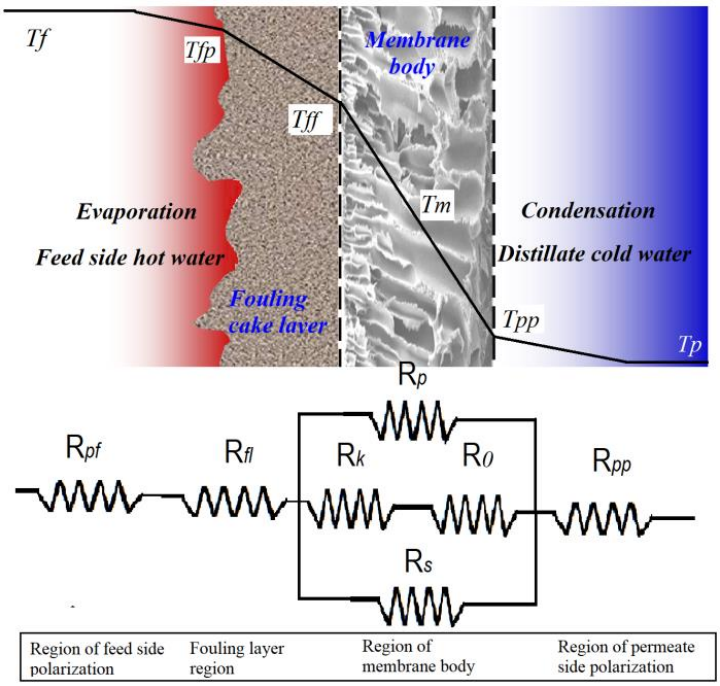

Fig.1. Typical electric circuit analogy of heat & mass resistance of fouled membrane

$$B = \frac{J_w}{\Delta P^0} = \frac{1}{1/B_{fb} + 1/B_{fl} + 1/B_m + 1/B_{pp}} \quad (1)$$

In the above **Fig. 1**, the mass transfer resistance induced by the permeate water concentration polarization (R_{pp}) surface diffusion mechanism (R_s) is ignored [24]. Among all suggested models so far, the dusty gas model shown below is widely implemented in MD to describe combinations of all these transport mechanisms, excluding surface diffusion [18,20,25,26].

$$J_i = J_i^D + J_i^V \quad (2)$$

$$\frac{J_i^D}{D_{ie}^k} + \sum_{j=1\neq i}^{n} \frac{p_j J_i^D - p_i J_j^D}{D_{ije}^0} = -\frac{1}{RT_m}\nabla p_i \quad (3)$$

$$J_i^v = -\frac{\varepsilon r^2 p_i}{8RT_m \tau \mu}\nabla P \quad (4)$$

$$D_{ie}^k = \frac{2\varepsilon r}{3\tau}\sqrt{\frac{8RT_m}{\pi M_i}} \quad (5)$$

$$D_{ije}^o = \frac{\varepsilon}{\tau} P D_{ij}^o \quad (6)$$

Where subscripts e and i refer to the effective diffusion coefficients and the transported compound i. T_m is the average membrane temperature. D^k and D^0 are the Knudsen and ordinary diffusion coefficients. J_i,J^D, and J^v

are the total, diffusive, and viscous flux values respectively. P, μ, r, ε, M, and τ are the total pressure, the viscosity of the gas mixture, the membrane pore radius, the porosity, the molecular weight, and the membrane tortuosity respectively. Hence, from **Eq. 2**, the general mass transport coefficient follows this equation [27].

$$B_i^m = \frac{N}{\delta}\left[\sum_{j=1}^{m(r=0.5\lambda)} G_i^K f_j r_j^3 + \sum_{j=m(r=0.5\lambda)}^{p(r=50\lambda)} \left(\frac{1}{G_i^K r_j} + \frac{1}{G_i^D}\right)^{-1} f_j r_j^2 + \sum_{j=p(r=50\lambda)}^{n(r=r_{max})} G_i^D f_j r_j^2\right] \quad (7)$$

where (8)

$$G_j^k = \left(\frac{32\pi}{9M_i RT_m}\right)^{1/2}$$

$$G_i^D = \left(\frac{\pi P D_i}{RT_m p_a}\right)^{1/2} \quad (9)$$

By eliminating pore size distribution effects and adopting tortuosity, a more simplified form of mass transfer coefficient for Knudsen (B_k), ordinary (B_o), Poiseuille(B_p),and combinations ($B_{ok/kp}$) can be established, as follows

$$B_k = 1.064\left(\frac{r\varepsilon}{\tau\delta}\right)\left(\frac{M_w}{RT_m}\right)^{0.5} \quad (10)$$

$$B_o = \frac{1}{Y_{lm}}\left(\frac{D_w\varepsilon}{\tau\delta}\right)\left(\frac{M_w}{RT_m}\right) \quad (11)$$

$$B_p = 0.125\left(\frac{r^2\varepsilon}{\tau\delta}\right)\left(\frac{M_w P_a}{\eta RT_m}\right) \quad (12)$$

$$B_{c\_OK} = \left(\frac{1}{\frac{Y_{lm}}{B_o} + \frac{1}{B_k}}\right) + B_p \quad (13)$$

$$B_{c\_KP} = \left(\frac{1}{\frac{1}{B_k}}\right) + B_p \quad (14)$$

$$\text{Where, } PD_w = 1.895*10^{-5}*T^{2.072} \quad (15)$$

$$T_m = \frac{T_{ff} - T_{pp}}{lnT_{ff} - lnT_{pp}} \quad (16)$$

$$Y_{lm} = \frac{Y_f - Y_p}{lnY_f - lnY_p} \quad (17)$$

where the PD_w = water air diffusivity (Pa.m^2/s), estimated from **Eq. 15**, and τ, δ, ε, and r are the membrane characteristics tortuosity, thickness (m), porosity, and pore diameter (m), respectively [28]. The membrane tortuosity of (τ=2) is often recommended [28,29]. Mw=water molecular weight, R = ideal gas constant, T=absolute temperature, T_m=log-mean temperature, T_{ff}=feed side membrane surface temperature, T_{pp}=permeate side membrane surface temperature, Y_{lm}=log-mean air fraction, and $Y_{f/p}$=air mole fractions on feed/permeate side, calculated from vapor pressure $P_{f/p}$.

3 Materials and methods

Commercially available hydrophobic membranes: Metricel 0.45 μm (PP04514225) and 0.1 μm (PP0114225) polypropylene (PP), Millipore - Durapore 0.22 & 0.45μm Polyvinylidenefluoride (PVDF) , and Millipore - Fluoropore 0.22 μm Polytetrafluoroethylene (PTFE) as indicated on [5] have been utilized for a bench scale DCMD cell having effective membrane area 0.0043 m^2, hydraulic radius 0.002 m^2, and channel dimensions 0.001 m (depth) X 0.07 m (length). The experiment was conducted at various velocities (0.5 - 2 L/min), with feed temperature in a range of 293 K to 333 K and pH of 7. The hot solution (shown in **Table 1**) was initially circulated through the feed side and cold deionized (DI) water was used on the permeate side. With this process, water vapor from the feed side is transported to the permeate side. The equipment utilized included a circulation pump (Cole Parmer Instrument, company model 75211-15, USA), heater (Lab companion BW10H heating bath), chiller (CPT Inc. refrigerated bath circulator, Republic of Korea), temperature and conductivity meter (WTW-Multi 3410, Germany), permeate water weighing meter (OHAUS-Explorer pro electronic digital balance, USA), pH meter (Thermo scientific Singapore Orion star series pH meter, Singapore), and digital pressure sensor to measure liquid entry pressure (10.00 bar, Autonics PSA-1, USA). SEM & EDX were conducted using high-resolution field emission scanning electron microscopy (FESEM) S-4300 SE (Hitachi, Tokyo, Japan) with a Q150T Turbo-Pumped sputter platinum coater (Quorum Technologies Ltd, UK). Deionized water was obtained from a multi-stage water purification process (Puris RO water system, Republic of Korea); chemicals utilized include NaF & NaOH (SHOWA, Japan), $CaCl_2$ (Kanto Chemical, Japan), $MgCO_3$ (Katayama chem., Japan), KNO_3, HCl, KH_2PO_4 (SAMCHUN chem., Korea), humic acid (HA) (ALDRICH, Switzerland), and $MnSO_4.H_2O$ (PAEJUNG Chem., Korea). Visual MINTEQ 3.1 chemical equilibrium model has been utilized toanalyze the saturation index and speciation; MATLAB has been employed for the modeling work, using the algorithm flow chart shown in **Fig. 2**

Table 1. Chemical composition of the used industrial wastewater sample in this study [5]

Cations / Anions	Ca^{2+}	Mg^{2+}	K^+	Na^+	Mn^{2+}	F^-	Cl^-	SO_4^{2-}	NO_3^-	CO_3^{2-}	$H_2PO_4^-$	SiO_2	Humic Acid
Conc. (mg/L)	75.5	76.18	9.64	605	4	1,000	134	229	15.5	55	9.4	1000	15

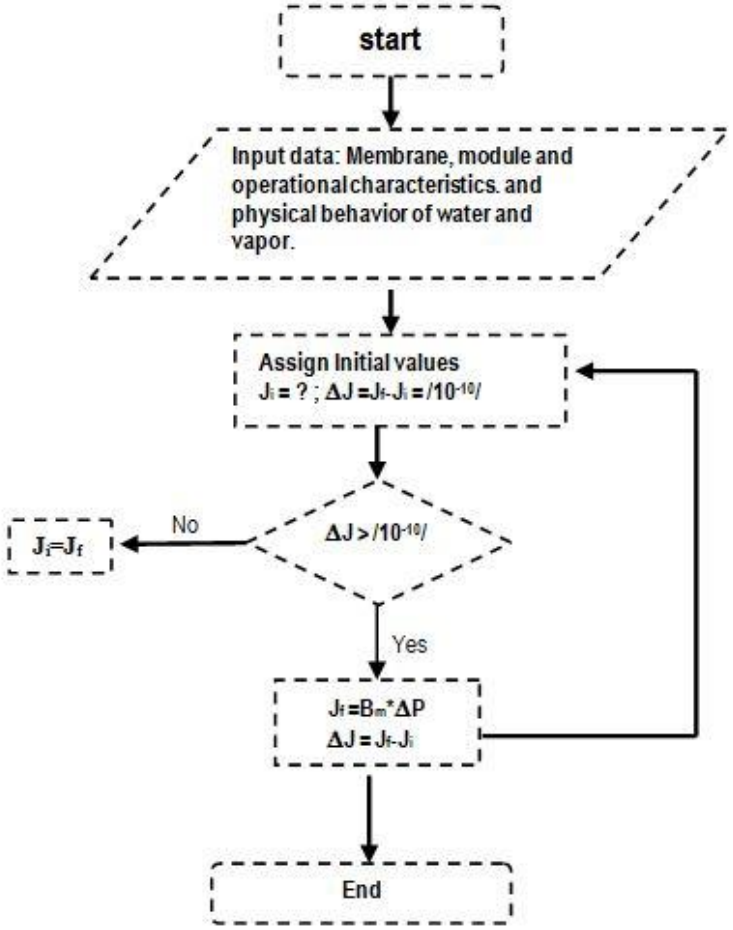

Fig.2. Algorithm flowchart for estimating mass flux of different models

4 Results and discussion

4.1 Mass transfer behavior of MD utilizing wastewater as a feed

As it has been discussed earlier, permeate flux decline in MD process is believed to emanate from heat transfer resistance and/or the direct hydraulic resistance from the fouling cake layer. In order to be clear with this controversy, four major phenomenon have been checked: presence of any kind of fouling, exact place of foulant's deposition (inside membrane or surface only), if flux decline is because of fouling or not, and whether the main reasons are both from heat and mass transfer resistance of the cake layer or not. Accordingly, over 15 h experiment was conducted using an industrial wastewater sample consisting of both organic and inorganic components (see **Table 1**). Different pore size (0.1 µm PP, 0.45 µm PP & 0.45 µm PVDF) membranes have been utilized. Experimental results revealed that, as compared to the stable flux trend of pure water (**Fig. 3)**, the fouled membrane exhibits an increasing mass resistance and flux decline (**Fig. 4**). It is obvious that flux decline and additional mass transfer resistance in the second case is caused mainly due to membrane fouling.

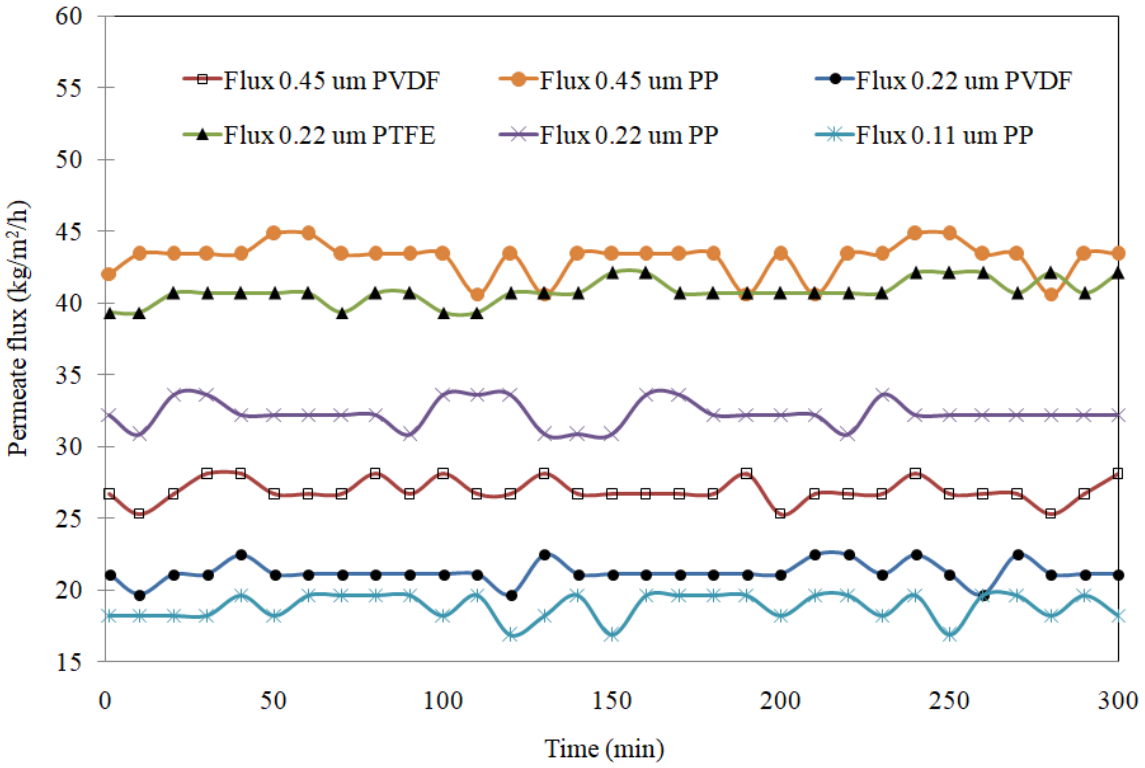

Fig. 3. Constant pure water flux through different membranes: (T_p = 293K;T_f= 333K; Q_f= Q_p =1L/min.)

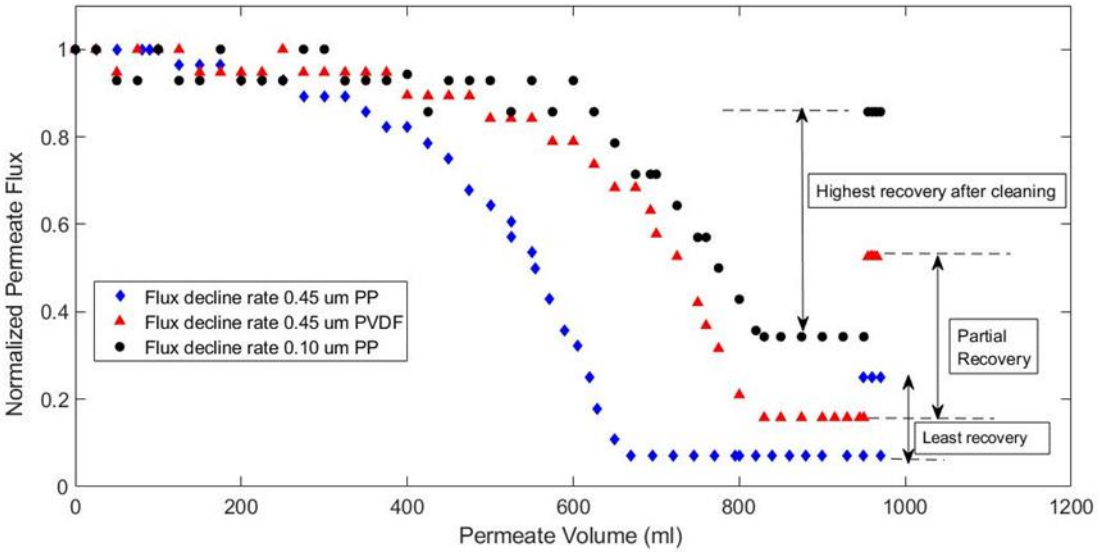

Fig. 4. Flux decline trend of different pore size membranes using wastewater as feed: *(T_p = 293K;T_f= 333K; Q_f= Q_p =1L/min. pH=7).* Initial flux of 0.1 µm PP, 0.45 µm PP and 0.45 µm PVDF was 19.7 kg/m^{2}h, 39.2 kg/m^{2}h and 26.1 kg/m^{2}h, respectively.

To confirm the formation of a fouling layer on the membrane surface, a visual inspection of dark brown cake on the membrane surface (**Fig. 5a**) and high-resolution SEM-EDX image analysis (**Fig. 5b-d**) has been utilized. Moreover, the saturation index (SI) from the Visual MINTEQ 3.1 software has also been checked and a value greater than 0 (see **Table 2**) was obtained, which indicates the higher tendency of the precipitated salts to deposit inside and on the membrane surface. It can be observed that as the VCF increases, the saturation index and type of the depositing mineral also varies owing to the withdrawal of water to the permeate side. The value of the SI being higher value shows very high chance of nucleation of different salts. The fundamental reason for the formation of fouling layer is the complex interaction between the ions in the feed wastewater and the humic acid molecules. Some of these are the shielding effect from Na^+ ion that coils the HA molecules, and the charge screening effect from the Ca^{2+} ion that tends to bind the carboxyl functional groups of the HA molecule [13]. These interactions will ultimately result in decreasing the electrostatic repulsion force and favors attachment of different objects to the membrane surface.

The humic acid in the wastewater sample and substantial amount of cementitious Ca^{2+} ion (as indicated by stoichiometric analysis and EDX image) aggravates the coagulation and adsorption of the inorganic salts on the membrane surface, inducing the formation of a thick cake layer [30].

Table 2. Saturation index and speciation analysis of the wastewater sample at pH 7

	Mineral	log IAP	SI	Stoichiometry			
VCF = 1							
1	FCO_3 apatite	-88.92	22.45	$9.32Ca^{2+}$	$0.36Na^{+}$	$0.15Mg^{2+}$	$4.8PO_4^{3-}$
2	Hydroxyapatite	-38.19	6.15	$5Ca^{2+}$	$3PO4^{3-}$	$1H_2O$	$-1H^{+}$
3	$MnHPO_4(s)$	-21.33	4.07	$1Mn^{2+}$	$1PO4^{3-}$	$1H^{+}$	
4	Fluorite	-6.23	4.05	$1Ca^{2+}$	$2F^{-}$		
5	Sepiolite	16.39	2.73	$2Mg^{2+}$	$3H_4SiO_4$	$-4H^{+}$	$-0.5H_2O$
VCF = 2.5							
1	FCO_3 apatite	-84.69	26.68	$9.32Ca^{2+}$	$0.36Na^{+}$	$0.144Mg^{2+}$	$4.8PO_4^{3-}$
2	Hydroxyapatite	-36.59	7.75	$5Ca^{2+}$	$3PO4^{3-}$	$1H_2O$	$-1H^{+}$
3	Fluorite	-5.37	4.91	$1Ca^{2+}$	$2F^{-}$		
4	$MnHPO_4(s)$	-20.95	4.45	$1Mn^{2+}$	$1PO4^{3-}$	$1H^{+}$	
5	Sepiolite	17.78	4.12	$2Mg^{2+}$	$3H_4SiO_4$	$-4H^{+}$	$-0.5H_2O$
VCF = 5							
1	FCO_3 aptite	-81.63	29.74	$9.32Ca^{2+}$	$0.36Na^{+}$	$0.144Mg^{2+}$	$4.8PO4^{3-}$
2	Hydroxyapatite	-35.45	8.88	$5Ca^{2+}$	$3PO4^{3-}$	$1H_2O$	$-1H^{+}$
3	Fluorite	-4.72	5.55	$1Ca^{2+}$	$2F^{-}$		
4	Sepiolite	18.86	5.19	$2Mg^{2+}$	$3H_4SiO_4$	$-4H^{+}$	$-0.5H_2O$
5	$MnHPO_4(s)$	-20.69	4.71	$1Mn^{2+}$	$1PO4^{3-}$	$1H^{+}$	

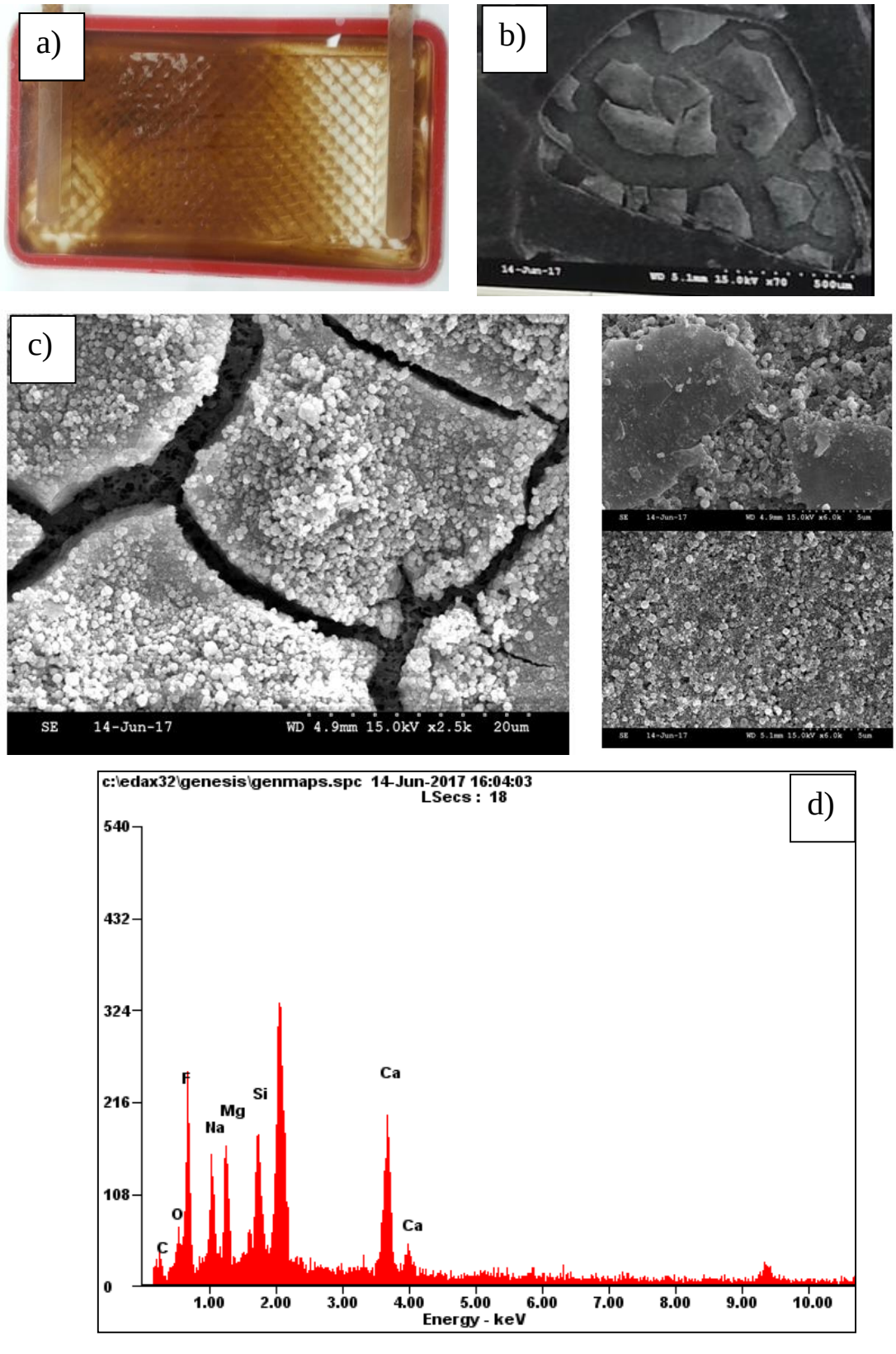

Fig. 5. SEM and EDX image of fouling layer on 0.1 µm PP membrane. (T_p = *293K;*T_f*= 333K;* Q_f*=* Q_p *=1L/min. pH=7.* a) Naked eye view of dark brown fouling cake layer on the membrane. b) 500 µm (15kv X 70) SEM image of fouled membrane surface. c) 5 and 20 µm SEM image showing both humic acid & inorganic salt accumulation d) EDX image: mineralogical composition of fouling layer on membrane surface

As indicated in **Fig. 4**, the flux decline resulted from the fouling cake layer on 0.45 μm PP membrane has shown a constant flux of 39.2 kg/m^2.h for only the first 35 min (8% recovery); However, 0.45 μm PVDF exhibited a constant value of 25.2 kg/m^2.h for 2 h until 24% recovery; then, this value tended to gently decrease until a final constant value of 4.09 kg/m^2.h. On the other hand, 0.10 μm PP persistently delivered a constant flux value of 18.20 kg/m^2.h for 9 h until 61% recovery; after this point the flux tended to decrease faster and reached a constant 6.72 kg/m^2.h value. This faster fouling in the membrane with larger pore size should probably be attributed to the deposition of particles both on the membrane surface and inside the pores, as larger pores have higher chance of being clogged from small size salt particle [5]. However, the adsorption and deposition of salt particle in the smaller size membrane (0.10 μm PP) are mainly significant on the membrane surface. The EDX and saturation index analysis have shown the presence of organic and inorganic deposition on the membrane surface: both high pH and low pH chemical cleaning is therefore required to remove the fouling layer [31,32]. A two-stage membrane cleaning experiment using low pH 0.5 % (w) HCl for 2 h, followed by high pH 0.1%(w) NaOH for 1 h (for removal of inorganic and organic matter, respectively) then confirmed the same in that chemical cleaning of the fouled membrane managed to recover the flux of 0.1 μm membrane to nearly 90.1%, but that of the 0.45 μm PVDF and 0.45 μm PP to only 62% and 42% respectively (see **Fig. 4**). The fundamental flux behavior difference between the two 0.45 μm pore size membranes (PVDF and PP) emanates mainly from their material type which directly affects their heat transfer tendency. Even though, both membranes have the same pore size, the other intrinsic behaviors (such as contact angle, surface roughness, porosity, LEP, and thickness) are different which leads to difference in their flux behavior [5]. This significant mass transfer resistance, persistent flux decline even after chemical cleaning, and lack of complete recovery of the membrane, emphasize the existence of substantial amounts of particles in the membrane pores. This magnitude is bigger for the larger pore size membrane than the smaller one. A similar case with $CaCO_3$ deposition inside the membrane pore has been observed elsewhere [14]. The easier and fast removal of fouling layer in the small pore size membrane is attributed to the deposition of most of the fouling matter on the membrane surface, as opposed to the case of the larger pore size membrane, where deposition also includes inside the membrane pores. Moreover, a higher wetting tendency of fluoride ion of up to 1.3 mg/L has also been observed in the larger pores size membrane, which supports the absorption and availability of a significant amount of feed side ions in the membrane pores. The fluoride wetting tendency is only 0.3 mg/L for the smaller pore size membrane. Even though, some researchers [13] believe that deposition of particles inside the MD membrane is not possible, this experiment and some other works [9,14] confirmed the possibility of deposition and its direct resistance on the mass transfer process.

Therefore, the flux decline phenomenon is generally attributed to the following reasons: In fouled membrane a significant portion of the pore entrances of the membrane are blocked by the deposit layer and this reduces surface area available for vaporization [13,33]. Secondly, the thickening of feed water (similar to concentration polarization) in the evaporation surface reduces the partial vapor pressure of water [33] and thirdly the fouling layer is an additional layer that increases the thickness of the path, ultimately resulting in an increase in mass resistance [34]. On the other hand, the fouling layer also reduces the flux by decreasing the heat transfer driving

force. This directly affects the heat transfer efficiency. Different researchers utilized temperature polarization coefficient (TPC) to measure the effect of the fouling cake layer on the flux deterioration [9,35,36]. In this study also the TPC for all the three membranes was significantly decreasing showing that the inefficient heat transfer mechanism also contributes to the flux decline in MD. This highlight that, pore size selection has bigger contribution in the mass transfer behavior. Another effect of membrane pore size in the mass transfer analysis is indicated in the next section.

4.2 Mass transfer behavior of MD utilizing pure water as a feed

4.2.1 Effect of membrane parameter on mass transfer behavior

The mass transfer in the MD membrane does not occur only through the diffusion mechanism. It is believed that there is also a significant contribution of Poiseuille flow to the process. An experiment has been undertaken on three different membranes using pure water to study if there is any contribution of Poiseuille flow to the overall mass transport through MD membrane. Accordingly, estimation of the permeate flux (**see Fig. 3**) and mass transfer coefficient (**see Fig. 6**) of different membranes have shown that the permeate flux of the PTFE 0.22 µm membrane is much higher than those of PVDF 0.22 µm and PVDF 0.45 µm, albeit the pore sizes are similar or even smaller. However, the mass transfer coefficient of PTFE 0.22 µm is smaller and decreases as compared to those of PVDF 0.22 µm and PVDF 0.45 µm, whose mass transfer coefficient increases with temperature.

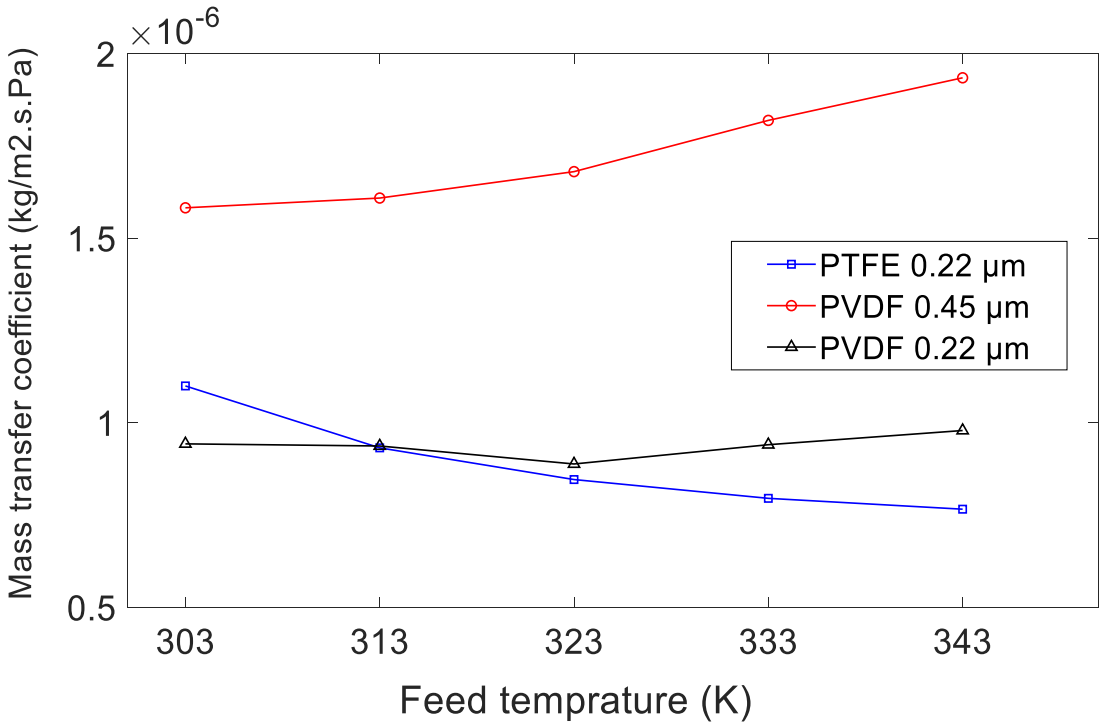

Fig. 6. Experimentally measured mass transfer coefficient for different membranes.

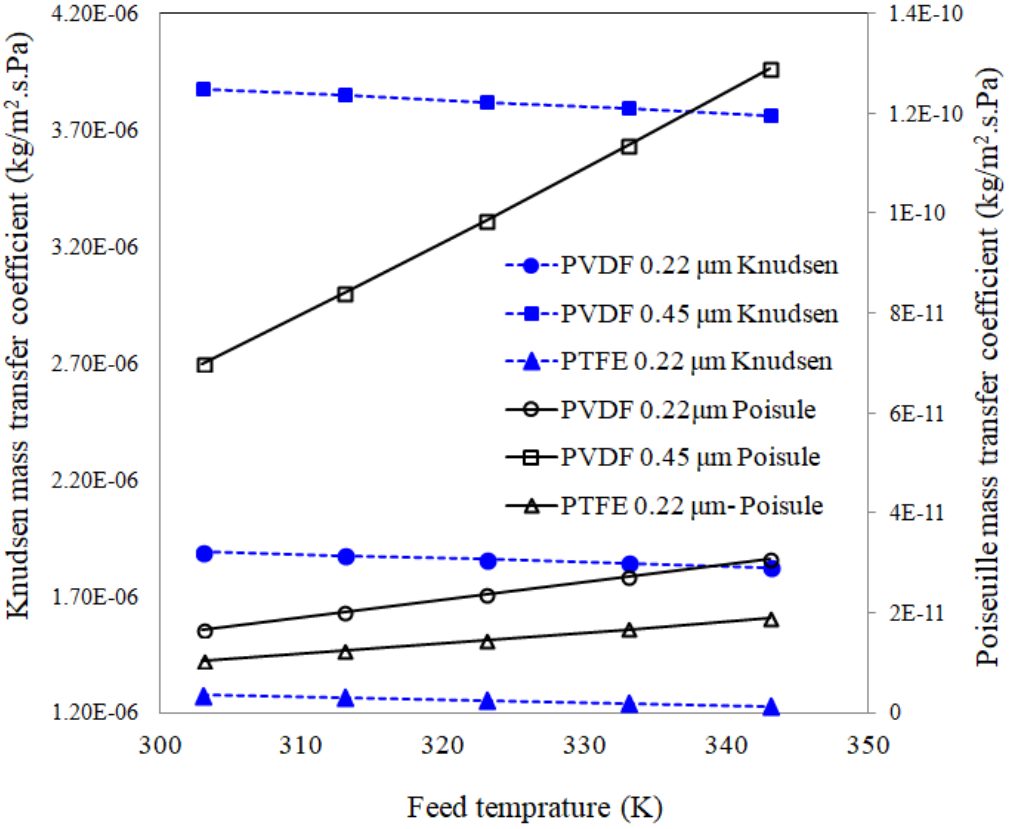

Fig. 7. Knudsen diffusion and Poiseuille flow variation with temperature.

This clearly indicates that the higher mass transfer in PTFE 0.22 µm is not from its mass transfer coefficient component; rather, it is from the heat and thermal efficiency, which exponentially elevated the partial vapor pressure difference. It should also be noticed that the decrease in mass transfer in PTFE 0.22 µm resulted from the significant and fast decline of the Knudsen diffusion component at higher temperature (see **Fig. 7**). Therefore, we can infer that those membranes having Knudsen diffusion as a dominant mass transfer coefficient will have a decreasing mass transfer coefficient. On the other hand, mass transfer increases in the PVDF 0.45 µm and 0.22 µm samples mainly confirm that the contribution of mass transfer by Knudsen diffusion is minimal and increase in mass transfer probably comes from the Poiseuille flow (see **Fig. 8**).

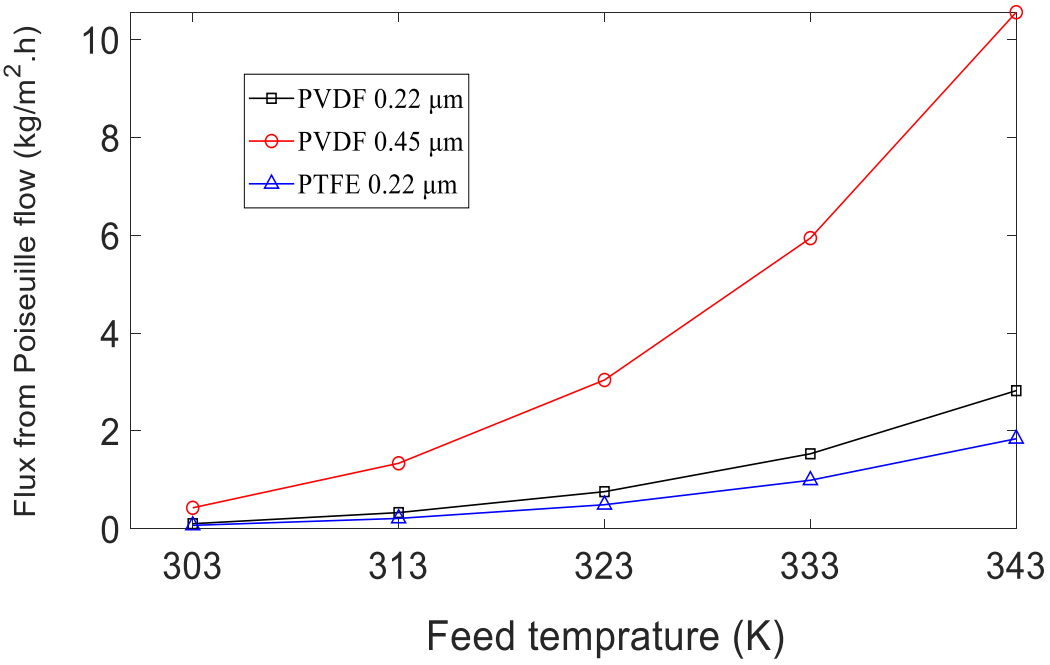

Fig. 8 Permeate flux from the Poiseuille flow contribution in different membranes.

In **Fig. 7** we can observe that as the temperature increases, the contribution of Poiseuille flow increases and that of Knudsen diffusion decreases. The Poiseuille flow contribution in the PVDF 0.45 µm sample is even larger and reaches up to 10.6 kg/m^2.h (see **Fig. 8**), which cannot be ignored in the MD mass transfer coefficient analysis. Other than the pore size, the effects of porosity and flow rate on Poiseuille flow dominance have also been checked. A substantial increase in the flow rate from 0.5 L/min to 4 L/min (from laminar to turbulent condition) was found not to significantly change the Poiseuille mass transfer coefficient (see **Fig. 9a**), while porosity significantly affects the permeate flux of membranes with larger pore size (see **Fig. 9b**). This can also be one of the reasons why Poiseuille flow is relatively higher for the0.45 µm size sample.

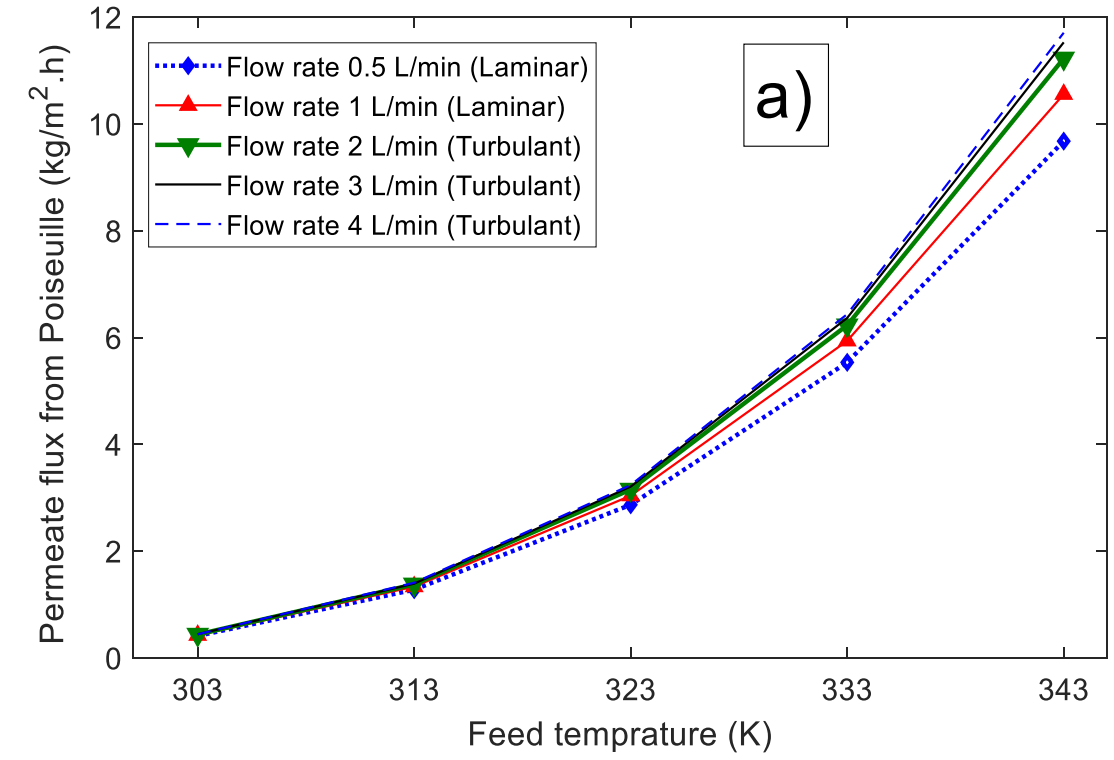

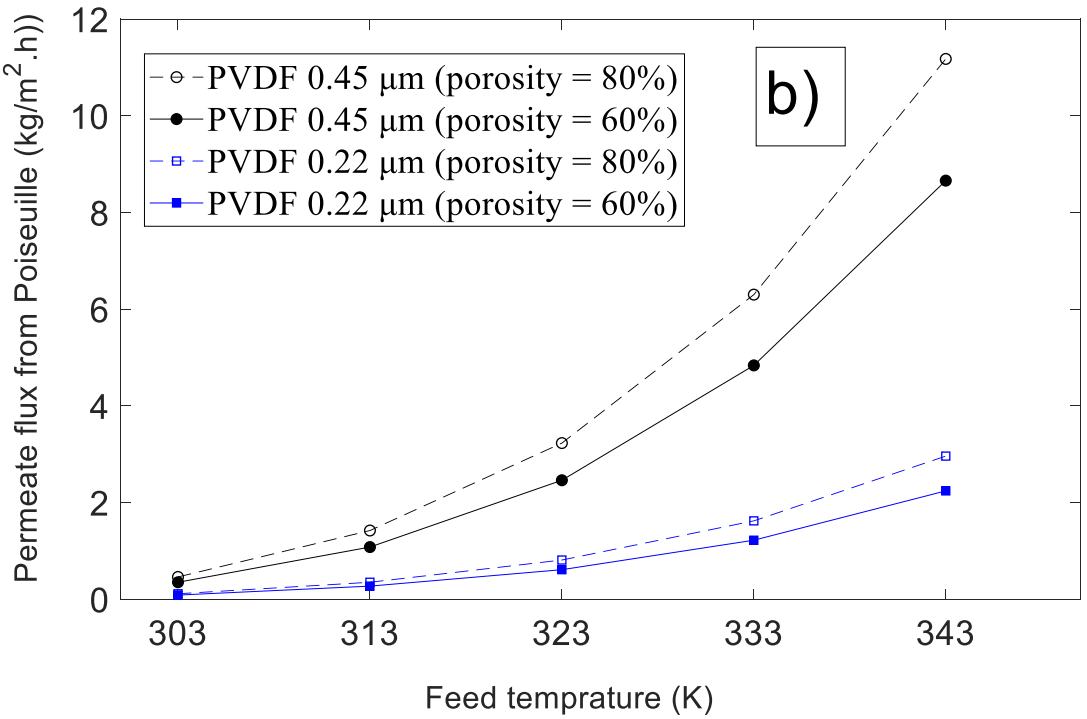

Fig. 9 a) Effect of flow rate on Poiseuille flow b) Effect of porosity on Poiseuille flow.

4.2.2 Dominant transport mechanisms in different membranes

The dominant mass transfer mechanism for each membrane has been identified by comparing the experimental results with those of the dusty gas equations mentioned earlier (see Eq. 10 - 14). All possible mass transport mechanisms in the membrane (Knudsen, molecular, and Poiseuille) and their possible combinations have been considered for the analysis using the MATLAB Software. Accordingly, the dominant mass transfer mechanism for the PVDF 0.22 µm and 0.45 µm samples was the combination of all the three process, the Knudsen, molecular, and Poiseuille (KMP) processes, which agrees with the results from [25]; the dominant mass transfer mechanism for the PTFE 0.22 µm sample is the combined Knudsen-Poiseuille model (KP) (refer to **Fig. 10** and **Table 3-5**). This result also agrees with several other previous works [21,37–39]. This significant mass transfer mechanism difference originates mainly from the variation in physical characteristics and the interaction with the water vapor molecules obtained as a result of different membrane material type use and fabrication methods, which resulted in differences of thickness, porosity, membrane roughness, and hydrophobicity. The PTFE membrane has a smaller membrane thickness, which affects the thermodynamic effects of the system and, in turn, could increase the flux. Higher porosity also favors higher permeate flux and lowers the conductive heat loss. The higher surface roughness reduces the boundary layer thickness, which increases the permeate flux. The higher roughness in PTFE also significantly reduces the wettability [15].

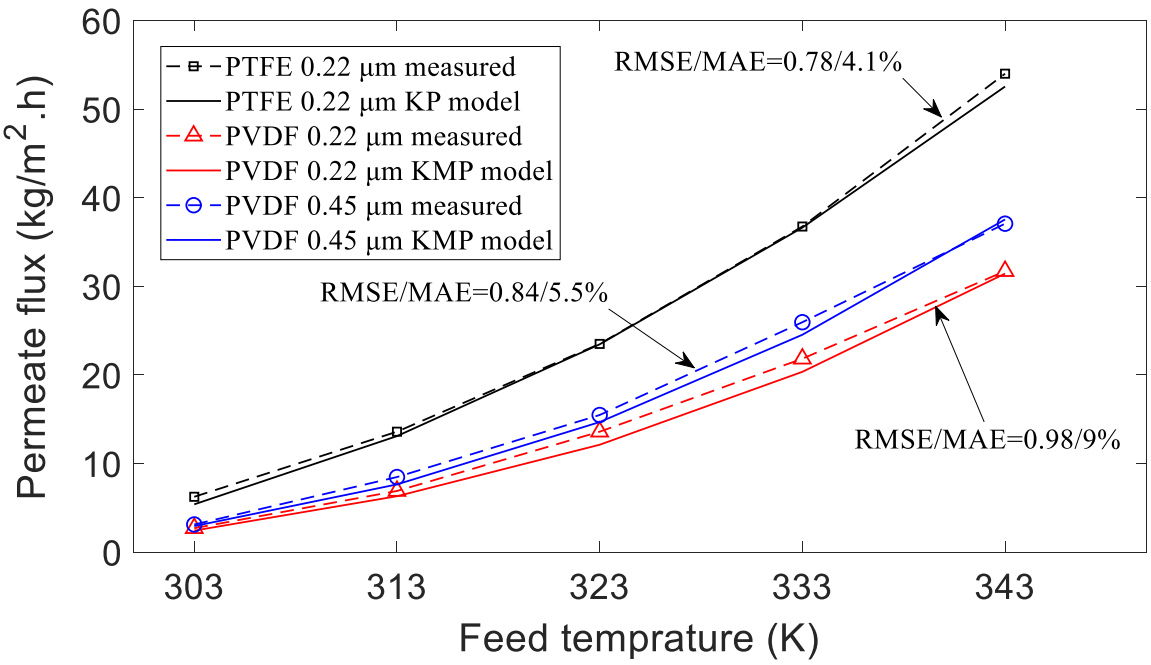

Fig. 10. Experimental vs. dominant mass transfer model comparison for different membrane types (Define RMSE, MAE, KMP, KP here).

Table 3. Comparison of experimental results for PVDF 0.22 μm with all mass transfer models

Permeate temp, K	Feed temp, K	Experimental	Knudsen	Molecular	Poiseuille	**KMP**	KM
293	303	2.70	7.03	2.94	0.10	**2.43**	2.36
293	313	6.90	16.49	7.57	0.33	**6.31**	6.09
293	323	13.59	28.45	14.40	0.76	**12.12**	11.66
293	333	21.83	42.76	23.96	1.53	**20.35**	19.55
293	343	31.71	59.11	36.65	2.82	**31.43**	30.21
Root mean square error (RMSE)			17.43	2.44	17.1	**0.98**	1.54
Mean absolute percentage error, (MAE), %			118.0	10.0	93.0	**7.0**	11.0

Table 4. Comparison of experimental results for PVDF 0.45 μm with all mass transfer models

Permeate temp, K	Feed temp, K	Experimental	Knudsen	Molecular	Poiseuille	KMP	KM
293	303	3.12	10.09	2.95	0.43	**2.93**	2.63
293	313	8.47	22.67	7.57	1.34	**7.64**	6.77
293	323	15.48	37.47	14.41	3.04	**14.68**	12.92
293	333	25.95	54.09	23.95	5.94	**24.53**	21.59
293	343	37.07	72.09	36.63	10.56	**37.55**	33.19
Root mean square error (RMSE)			23.46	1.11	16.22	**0.84**	2.95
Mean absolute percentage error (MAE), %			147.0	6.4	79.9	**5.5**	15.9

Table 5. Comparison of experimental results for PTFE 0.22 μm with all mass transfer models

Permeate temp, K	Feed temp, K	Experimental	Knudsen	Molecular	Poiseuille	KMP	KM	KP
293	303	6.24	5.40	2.31	0.07	1.86	1.81	**5.39**
293	313	13.59	13.02	6.06	0.21	4.90	4.74	**13.09**
293	323	23.50	23.31	11.83	0.49	9.60	9.28	**23.46**
293	333	36.75	36.40	20.33	0.99	16.60	16.00	**36.63**
293	343	54.00	52.22	32.38	1.84	26.57	25.62	**52.55**
Root mean square error (RMSE)			0.93	13.75	30.81	17.01	17.52	**0.78**
Mean absolute percentage error			4.60	50.60	97.80	59.80	61.10	**4.10**

(MAE), %

4.3 Effect of transmembrane thermal gradient on mass transfer

4.3.1 Non-isothermal condition and its applications

The magnitude of permeate mass flux in MD not only depends on the arithmetic transmembrane temperature gradient, but also on the individual values of permeate and feed side temperature, as the same temperature difference from different feed-permeate combinations can provide a significant, exponential difference in permeate yield. The PTFE 0.22 μm membrane has been utilized for its quick response to smaller temperatures changes. Accordingly, it is observed that, the same amount of permeate flux can be obtained from different transmembrane thermal gradients (see **Fig. 11 a-c**). Higher flux is obtained for combinations of higher feed temperature and lower permeates temperature. This is because higher feed temperature induces higher vapor production [40]. Even when the transmembrane gradient is equal, permeate temperature in a higher temperature range induces a higher vapor pressure force to counter the feed vapor pressure, and feed temperature in a lower temperature range does not generate enough vapor, resulting in less mass flux. Mass flux depends more on the amount of vapor produced than on simply the arithmetic transmembrane temperature gradient. An isoflux contour plot from the experimental data (**Fig. 11b**) and from the dusty gas based theoretical estimation (**Fig. 11c**) has been developed to ease selection of the optimum operating temperature for specific permeate yield. This methodology can be easily applied to select the best operating feed/permeate temperature combination fitting our water demand (permeate yield) and climate condition (room temperature) in actual large-scale MD-based desalination and wastewater treatment processes.

In addition to the higher permeate flux, utilizing higher feed temperature also significantly aids in reducing the wettability of the membrane. Concentration of fluoride ion on the permeate side has been utilized as a means to study the wetting performance of the membrane at different feed temperatures. Accordingly, **Fig. 11d** shows that for the same transmembrane temperature gradient, a combination of higher feed and lower permeate temperature can provide lower wetting rate, and vice versa. This is because a higher temperature combination produces a substantial amount of vapor, so that even with a lower transmembrane gradient there will be higher vapor mass transport, which obscures the solute transport effect with the dilution effect. Moreover, as the availability of vapor in the module increases, the membrane gives higher priority to vapor transport than to solute or solvent transport, so that the rates of migration of the solute and solvent will be minimal. Therefore, higher operating feed temperature and lower permeate temperature are better options as far as permeate water quality is concerned.

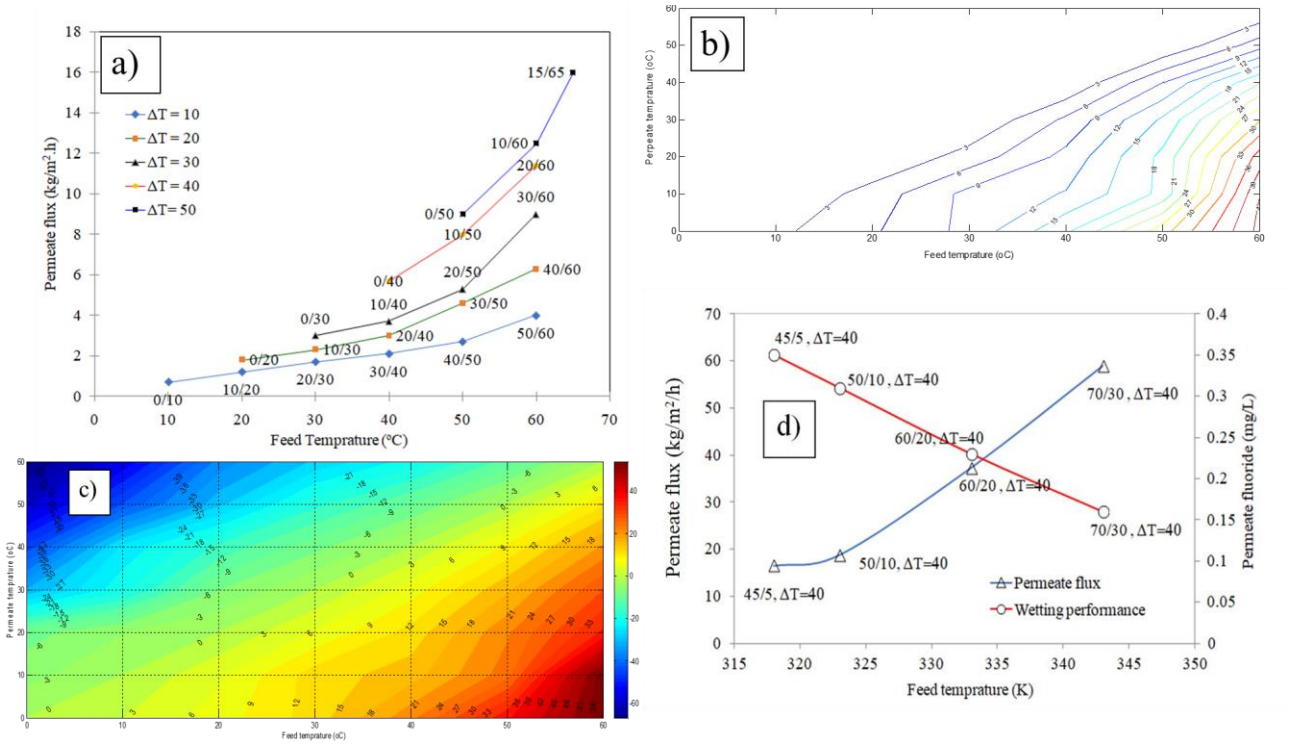

Fig. 11 a) Variation of permeate mass flux for the same temperature gradient *(Operation condition: Q_f= Q_p =1 L/min.; membrane type = PTFE 0.22 um).* b) Experimental isoflux contour plot for different feed and permeate temperature combinations*(Operation condition Q_f= Q_p =1 L/min.; membrane type = PTFE 0.22 um).* c) Dusty gas based theoretical isoflux contour plot for different feed/permeate temperature combinations (membrane type PTFE 0.22um;*Q_f= Q_p =1 L/min).* d) Permeate mass flux and wetting performance for different feed and permeate combinations *(membrane type PTFE 0.22 um; Q_f= Q_p =1 L/min. ΔT=40 K, fluoride concentration = 1,000 mg/L, pH=7)/*

4.3.2 Isothermal conditions and low operating temperatures

For lower feed/permeate temperature combinations (< 10^0C e.g [10/0]) and for any zero transmembrane thermal gradient (isothermal condition), interestingly, the permeate flux is never zero, as there is always a minimum back and forth flow, ranging from 4.2 to 6.4 kg/m^2.h,based on the membrane type **(Fig. 12)**. This clearly shows that permeate flux does not exclusively depend on the transmembrane gradient; rather, there is also a very small contribution from direct solvent transport. This is attributable to the higher tendency of solvent to pass through the larger membrane pores induced as a result of suppressed vapor production in the feed water. This minimal flow is not vapor diffusion; it is rather migration of direct water molecules, and is responsible for the initial partial wetting in the MD plant operation. The continuous extended time operation of the system under this condition even worsens the wetting rate (by increasing fluoride ion migration from 0.29 mg/L to 1.51 mg/L) as a result of the bridging effect and membrane damage [41]. The same result has been reported elsewhere [42]. This operational isothermal condition was also taken as an opportunity to study the direct effect of flow rate on the mass transport. Accordingly, increasing the flow rate of the feed side (from

1 L/min to 2.5 L/min) under isothermal condition affected neither the minimal flow nor the partial wetting tendency, which leads to the conclusion that flow rate did not have any direct impact in pushing the water or vapor molecules through the MD pore mouth; rather, it facilitates a flux increment only by improving the system hydrodynamic condition through enhancing thermal efficiency by increasing Reynolds number which ultimately alter the interfacial temperature polarization and concentration polarization effects [26,43].

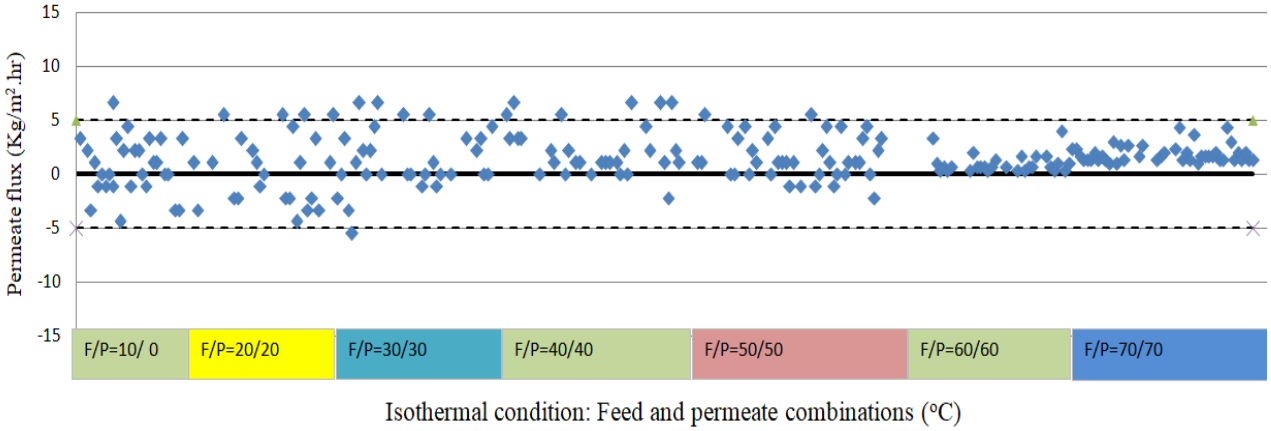

Fig. 12 Permeate flux under isothermal condition *(membrane type PTFE 0.22 um; Q_p =1 L/min., $\Delta T=^0C$ K, fluoride concentration = 1,000 mg/L, pH=7).*

5 Concluding remarks

Brief research objectives should have addressed at the first sentence. Mass transport resistance and flux decline in MD are results of both heat and mass transfer resistance. The fouling layer affects flux directly by resisting mass transport and indirectly by decreasing the heat transfer mechanism. Different membranes have different levels of heat transfer efficiency. Inefficient heat transfer thus reduces the partial pressure, which ultimately results in flux decline. Direct mass transfer resistance emanates from the cake layer on the membrane surface and from particles adsorbed in the membrane pores. In large pore size membranes, larger amounts of particles can be accumulated in the membrane pores. Membrane parameters have a significant effect on the mass transfer analysis; hence, these parameters have to be considered in designing a MD process. The PTFE membrane has superior mass transfer efficiency compared to the PVDF membrane, due to its intrinsic membrane behavior. In MD, consideration of Poiseuille flow for mass transfer analysis is essential, as it significantly contributes to the mass transfer mechanism. Its contribution is even larger at higher temperatures and for larger pore size membranes. For simulation and analysis of mass transfer resistance, it is also essential to consider different membrane parameters, such as pore size. This study also provides systematic insight in to the development of a strategy to select the appropriate operating feed/permeate temperature fitting for water demand and environmental conditions from an ‘isoflux’ plot for a MD plant. However, to reinforce the conclusions, these results have to be reinvestigated for different modules, membranes, and operating characteristics. Additional points are:

- Mass flux more strongly depends on the amount of vapor produced in the system than on just an arithmetic temperature difference between the two sides;

- Higher operating temperatures are preferred for both flux and wetting aspects;
- Transmembrane temperature gradient is not the only reason for mass transport (liquid & vapor) to the permeate side, as there might always be some minimum amount of non-vapor solute and solvent transport through larger membrane pore mouth by partial wetting;
- Mass transfer (of vapor) is mainly due to transmembrane gradient; the effect of flow rate on the flux is only indirect through enhancing of the thermal efficiency by increasing the Reynolds number and improving the overall hydrodynamic condition. The flow rate did not even have an effect on the liquid flow during the occurrence of partial wetting phenomenon.

ACKNOWLEDGEMENT

This research was supported by UST (Daejeon) and a grant (code 17IFIP-B065893-05) from Industrial Facilities & Infrastructure Research Program funded by Ministry of Land, Infrastructure, and Transport of Korean government.

REFERENCE

[1] Q.-M. Nguyen, S. Jeong, S. Lee, Characteristics of membrane foulants at different degrees of SWRO brine concentration by membrane distillation, Desalination. 409 (2017) 7–20. doi:10.1016/j.desal.2017.01.007.

[2] A. Alkhudhiri, N. Darwish, N. Hilal, Membrane distillation: A comprehensive review, Desalination. 287 (2012) 2–18. doi:10.1016/j.desal.2011.08.027.

[3] S. Goh, J. Zhang, Y. Liu, A.G. Fane, Fouling and wetting in membrane distillation (MD) and MD-bioreactor (MDBR) for wastewater reclamation, Desalination. 323 (2013) 39–47. doi:10.1016/j.desal.2012.12.001.

[4] M. Laqbaqbi, J.A. Sanmartino, M. Khayet, C. García-Payo, M. Chaouch, Fouling in Membrane Distillation, Osmotic Distillation and Osmotic Membrane Distillation, Appl. Sci. 7 (2017) 334. doi:10.3390/app7040334.

[5] M.M. Damtie, B. Kim, Y.C. Woo, J.-S. Choi, Membrane distillation for industrial wastewater treatment: Studying the effects of membrane parameters on the wetting performance, Chemosphere. 206 (2018) 793–801. doi:10.1016/j.chemosphere.2018.05.070.

[6] S. Goh, J. Zhang, Y. Liu, A.G. Fane, Fouling and wetting in membrane distillation (MD) and MD-bioreactor (MDBR) for wastewater reclamation, Desalination. 323 (2013) 39–47. doi:10.1016/j.desal.2012.12.001.

[7] E. Curcio, X. Ji, G. Di Profio, A.O. Sulaiman, E. Fontananova, E. Drioli, Membrane distillation operated at high seawater concentration factors: Role of the membrane on CaCO3 scaling in presence of humic acid, J. Membr. Sci. 346 (2010) 263–269. doi:10.1016/j.memsci.2009.09.044.

[8] Y.Z. Tan, J.W. Chew, W.B. Krantz, Effect of humic-acid fouling on membrane distillation, J. Membr. Sci. 504 (2016) 263–273. doi:10.1016/j.memsci.2015.12.051.

[9] M. Gryta, Fouling in direct contact membrane distillation process, J. Membr. Sci. 325 (2008) 383–394. doi:10.1016/j.memsci.2008.08.001.

[10] J. Phattaranawik, A.G. Fane, A.C.S. Pasquier, W. Bing, F.S. Wong, Experimental Study and Design of a Submerged Membrane Distillation Bioreactor, Chem. Eng. Technol. 32 (n.d.) 38–44. doi:10.1002/ceat.200800498.

[11] J.W. Chew, W.B. Krantz, A.G. Fane, Effect of a macromolecular- or bio-fouling layer on membrane distillation, J. Membr. Sci. 456 (2014) 66–76. doi:10.1016/j.memsci.2014.01.025.

[12] G. Naidu, S. Jeong, S.-J. Kim, I.S. Kim, S. Vigneswaran, Organic fouling behavior in direct contact membrane distillation, Desalination. 347 (2014) 230–239. doi:10.1016/j.desal.2014.05.045.

[13] S. Srisurichan, R. Jiraratananon, A.G. Fane, Humic acid fouling in the membrane distillation process, Desalination. 174 (2005) 63–72. doi:10.1016/j.desal.2004.09.003.

[14] M. Gryta, Influence of polypropylene membrane surface porosity on the performance of membrane distillation process, J. Membr. Sci. 287 (2007) 67–78. doi:10.1016/j.memsci.2006.10.011.

[15] M.M. Damtie, J.-S. Choi, Modeling and application of direct contact membrane distillation for fluoride removal from aqueous solutions, DESALINATION WATER Treat. 97 (2017) 23–40. doi:10.5004/dwt.201x.21690.

[16] M. Ramezanianpour, M. Sivakumar, An analytical flux decline model for membrane distillation, Desalination. 345 (2014) 1–12. doi:10.1016/j.desal.2014.04.006.

[17] Y.-L. Cheng, D.-J. Lee, J.-Y. Lai, Filtration blocking laws: Revisited, J. Taiwan Inst. Chem. Eng. 42 (2011) 506–508. doi:10.1016/j.jtice.2010.09.004.

[18] I. Hitsov, T. Maere, K. De Sitter, C. Dotremont, I. Nopens, Modelling approaches in membrane distillation: A critical review, Sep. Purif. Technol. 142 (2015) 48–64. doi:10.1016/j.seppur.2014.12.026.

[19] H. Ahadi, J. Karimi-Sabet, M. Shariaty-Niassar, T. Matsuura, Experimental and numerical evaluation of membrane distillation module for oxygen-18 separation, Chem. Eng. Res. Des. 132 (2018) 492–504. doi:10.1016/j.cherd.2018.01.042.

[20] M. Khayet, Membranes and theoretical modeling of membrane distillation: A review, Adv. Colloid Interface Sci. 164 (2011) 56–88. doi:10.1016/j.cis.2010.09.005.

[21] R.W. Schofield, A.G. Fane, C.J.D. Fell, Gas and vapour transport through microporous membranes. I. Knudsen-Poiseuille transition, J. Membr. Sci. 53 (1990) 159–171. doi:10.1016/0376-7388(90)80011-A.

[22] A.F. Ismail, T. Matsuura, Membrane Technology for Water and Wastewater Treatment, Energy and Environment, CRC Press, 2016.

[23] E. Drioli, A. Criscuoli, E. Curcio, Membrane Distillation and Osmotic Distillation, Membr. Sci. Technol. 11 (2006) 186–253. doi:10.1016/S0927-5193(05)80007-5.

[24] A. Alkhudhiri, N. Darwish, N. Hilal, Membrane distillation: A comprehensive review, Desalination. 287 (2012) 2–18. doi:10.1016/j.desal.2011.08.027.

[25] Z. Ding, R. Ma, A.G. Fane, A new model for mass transfer in direct contact membrane distillation,

Desalination. 151 (2003) 217–227. doi:10.1016/S0011-9164(02)01014-7.

[26] Y.M. Manawi, M. Khraisheh, A.K. Fard, F. Benyahia, S. Adham, Effect of operational parameters on distillate flux in direct contact membrane distillation (DCMD): Comparison between experimental and model predicted performance, Desalination. 336 (2014) 110–120. doi:10.1016/j.desal.2014.01.003.

[27] M. Khayet, A. Velázquez, J.I. Mengual, Modelling mass transport through a porous partition: Effect of pore size distribution, J. Non-Equilib. Thermodyn. 29 (2005) 279–299. doi:10.1515/JNETDY.2004.055.

[28] M. Khayet, T. Matsuura, Membrane Distillation: Principles and Applications, Elsevier, OXFORD, UK, 2011.

[29] A. Ali, F. Macedonio, E. Drioli, S. Aljlil, O.A. Alharbi, Experimental and theoretical evaluation of temperature polarization phenomenon in direct contact membrane distillation, Chem. Eng. Res. Des. 91 (2013) 1966–1977. doi:10.1016/j.cherd.2013.06.030.

[30] S. Srisurichan, R. Jiraratananon, A.G. Fane, Mass transfer mechanisms and transport resistances in direct contact membrane distillation process, J. Membr. Sci. 277 (2006) 186–194. doi:10.1016/j.memsci.2005.10.028.

[31] L.D. Tijing, Y.C. Woo, J.-S. Choi, S. Lee, S.-H. Kim, H.K. Shon, Fouling and its control in membrane distillation—A review, J. Membr. Sci. 475 (2015) 215–244. doi:10.1016/j.memsci.2014.09.042.

[32] Y. Wu, Y. Kang, L. Zhang, D. Qu, X. Cheng, L. Feng, Performance and fouling mechanism of direct contact membrane distillation (DCMD) treating fermentation wastewater with high organic concentrations, J. Environ. Sci. (2017). doi:10.1016/j.jes.2017.01.015.

[33] M. Gryta, M. Tomaszewska, J. Grzechulska, A.W. Morawski, Membrane distillation of NaCl solution containing natural organic matter, J. Membr. Sci. 181 (2001) 279–287. doi:10.1016/S0376-7388(00)00582-2.

[34] A. Hausmann, P. Sanciolo, T. Vasiljevic, U. Kulozik, M. Duke, Performance assessment of membrane distillation for skim milk and whey processing, J. Dairy Sci. 97 (2014) 56–71. doi:10.3168/jds.2013-7044.

[35] S.T. Hsu, K.T. Cheng, J.S. Chiou, Seawater desalination by direct contact membrane distillation, Desalination. 143 (2002) 279–287. doi:10.1016/S0011-9164(02)00266-7.

[36] S. Srisurichan, R. Jiraratananon, A.G. Fane, Humic acid fouling in the membrane distillation process, Desalination. 174 (2005) 63–72. doi:10.1016/j.desal.2004.09.003.

[37] M. Bhattacharya, S.K. Dutta, J. Sikder, M.K. Mandal, Computational and experimental study of chromium (VI) removal in direct contact membrane distillation, J. Membr. Sci. 450 (2014) 447–456. doi:10.1016/j.memsci.2013.09.037.

[38] T.-C. Chen, C.-D. Ho, H.-M. Yeh, Theoretical modeling and experimental analysis of direct contact membrane distillation, J. Membr. Sci. 330 (2009) 279–287. doi:10.1016/j.memsci.2008.12.063.

[39] L. Martínez, F.J. Florido-Díaz, A. Hernández, P. Prádanos, Characterisation of three hydrophobic porous membranes used in membrane distillation, J. Membr. Sci. 203 (2002) 15–27.

doi:10.1016/S0376-7388(01)00719-0.

[40] E. Jang, S.-H. Nam, T.-M. Hwang, S. Lee, Y. Choi, Effect of operating parameters on temperature and concentration polarization in vacuum membrane distillation process, Desalination Water Treat. 54 (2015) 871–880. doi:10.1080/19443994.2014.952673.

[41] E. Guillen-Burrieza, M.O. Mavukkandy, M.R. Bilad, H.A. Arafat, Understanding wetting phenomena in membrane distillation and how operational parameters can affect it, J. Membr. Sci. 515 (2016) 163–174. doi:10.1016/j.memsci.2016.05.051.

[42] R.B. Saffarini, B. Mansoor, R. Thomas, H.A. Arafat, Effect of temperature-dependent microstructure evolution on pore wetting in PTFE membranes under membrane distillation conditions, J. Membr. Sci. 429 (2013) 282–294. doi:10.1016/j.memsci.2012.11.049.

[43] L.M. Camacho, L. Dumée, J. Zhang, J. Li, M. Duke, J. Gomez, S. Gray, Advances in Membrane Distillation for Water Desalination and Purification Applications, Water. 5 (2013) 94–196. doi:10.3390/w5010094.